Dyes and Pigments 94 (2012) 74–80

Contents lists available at SciVerse ScienceDirect

Dyes and Pigments

journal homepage: www.elsevier.com/locate/dyepig

Controllable luminescence and electrochemical detection of Pb^{2+} ion based on the 2,2′-Azino-bis(3-ethylbenzothiazoline-6-sulfonate) dye and dodecanesulfonate co-intercalated layered double hydroxide

Jing Xu, Dongpeng Yan, Shuangde Li, Jun Lu*

State Key Laboratory of Chemical Resource Engineering, Beijing University of Chemical Technology, Beijing 100029, PR China

ARTICLE INFO

Article history:
Received 25 April 2011
Received in revised form
20 September 2011
Accepted 13 November 2011
Available online 27 November 2011

Keywords:
Luminescent dye
Organic–inorganic hybrid materials
Layered double hydroxide
Polarized fluorescence
Electrochemical response
2,2′-Azino-bis(3-ethylbenzothiazoline-6-sulfonate) anion

ABSTRACT

2,2′-Azino-bis(3-ethylbenzothiazoline-6-sulfonate) dye (ABTS) and dodecanesulfonate anion (SDS) have been co-intercalated into the ZnAl-layered double hydroxide (ZnAl LDH) matrix by a hydrothermal co-precipitation method, with obtained samples denoted as ABTS–SDS(x)/LDH (x stands for the molar percentage content of ABTS with respect to total intercalated content). The structure and chemical composition of the as-prepared compounds were characterized by X-ray diffraction (XRD), FT-IR spectra and elemental analysis. Fluorescence spectra demonstrated that the sample with 60% ABTS molar percentage, exhibited the optimal luminescent intensity. The fluorescence lifetime of ABTS in the gallery of LDH was enhanced significantly compared with that of pristine ABTS powder. As well, the ABTS–SDS/LDH thin film fabricated by the solvent evaporation method exhibited a well-defined c-orientation, which can be confirmed by XRD and scanning electron microscopy (SEM). Moreover, the ABTS–SDS(60%)/LDH film showed polarized luminescence (anisotropy: 0.35) and electrochemical response to aqueous solution containing Pb^{2+} ion. These results demonstrate that the ABTS–SDS/LDH system can serve as a good candidate for the solid-sate luminescence and electrochemical sensor materials.

1. Introduction

During last few years, considerable interest has been focused on the fabrication of photofunctional inorganic/organic hybrid materials because of their potential applications in the fields of light-emitting diodes [1], non-linear optics [2], sensors [3] and polarized devices [4]. The assembly of organic fluorescent dyes into inorganic host matrices (such as zeolites [5] and clay [6]) have been an important way to construct host–guest hybrid materials, which are considered as good candidates for solid-state dye laser [7] and luminescent materials [8]. In this regard, layered double hydroxides (LDHs), also known as "anionic clay" compounds, are one important family of such solid host matrices, which can be represented by the general formula $[M^{II}_{1-x}M^{III}_{x}(OH)_2]^{x+}A^{n-}_{x/n}\cdot yH_2O$. M^{II} and M^{III} are divalent and trivalent metals respectively; A^{n-} is the anion between the brucite-like layers to compensate for the positive charge [9–11]. The LDHs exhibit a large range of electronic [12] and magnetic properties [13], and they also play an important role in the fields of separation process [14], catalysis [15,16], controlled release of drug molecules [17] as well as functional nanostructures [18–21]. Moreover, the construction of LDHs-based luminescent materials have attracted much attention, since these organic–inorganic hybrid materials can show special physical and chemical characteristics which are not present in the individual components alone [22,23].

Recently, several luminescent dye molecules, such as pyrene [24], perylene [25], and rhodamine B chromophores [26], incorporated into LDHs systems were developed. The results show that the immobilized dye molecules can exhibit novel photophysical behavior in a confined and stable microenvironment [27], which is absent in solution and also favorable for their application as solid-state light-emitting materials. Furthermore, the host–guest interaction (such as the electrostatic, H-bond and van der Waals interaction) can facilitate a homogeneous distribution of the dye molecules in the galleries of LDH at the molecular level. Last but not least, the LDH matrix provides a higher mechanical and thermal stability for the dye molecules as well as reduces the environmental pollution and operational risk, which can meet the need of next generation luminescent materials [28].

2,2′-Azino-bis(3-ethylbenzothiazoline-6-sulfonate) anion with two sulfonate and several electron-donating groups (Fig. 1, donated as ABTS), is a well-known dye molecule, which is largely used in the

* Corresponding author. Tel.: +86 10 64412131; fax: +86 10 64425385.
E-mail address: lujun@mail.buct.edu.cn (J. Lu).

0143-7208/$ – see front matter © 2011 Elsevier Ltd. All rights reserved.
doi:10.1016/j.dyepig.2011.11.004

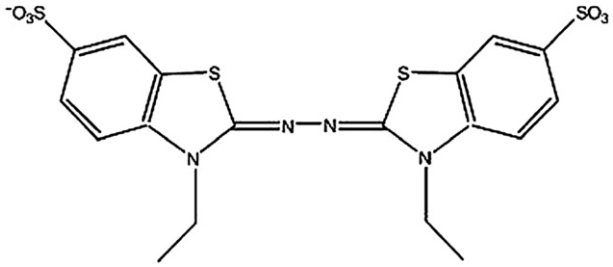

Fig. 1. The chemical structure of 2,2′-Azino-bis(3-ethylbenzothiazoline-6-sulfonate) (ABTS).

field of fluorescent brighter and colorimetric analysis. It has also received attention on the detection of chemical oxidants in the fields of environmental [29] and food science [30]. Therias et al. has reported that ABTS intercalated into the LDHs interlayer remain reversible redox active, compared with that of the pure ABTS [31]. To the best of our knowledge, however, the tunable photoemission behavior and the ion-detection property of ABTS assembled anion clays have never been reported. Herein, ABTS and 1-dodecanesulfonate (SDS) with different molar ratios co-intercalated into the LDHs were synthesized. The employment of SDS is to provide the ABTS molecule with a homogeneous nonpolar environment so as to prevent its aggregation and thus enhance the photoemission properties. Additionally, a confined and stable environment for the immobilization of ABTS molecules is offered by the LDH solid matrix, which further improve the preferred orientation of interlayer ABTS guests and facilitate the enhancement of the electrochemical signal effectively. Furthermore, the ABTS–SDS/LDH thin film was prepared by a solvent evaporation method, which exhibit well-defined polarized photoemission (fluorescence anisotropy: 0.35) and electrochemical activity. Therefore, this work not only demonstrates that the co-intercalation method is a feasible approach to prevent dye aggregation and to enhance its luminescence efficiency, but also provides a detailed understanding on the polarization photoemission characteristics for dye intercalated LDH systems. Moreover, we have also studied the application of the ABTS–SDS/LDH thin films in the detection of Pb^{2+} aqueous solutions by an electrochemical method. It can be expected that ABTS intercalated LDH system can serve as new type of organic–inorganic fluorescent material and electrochemical ion-probe.

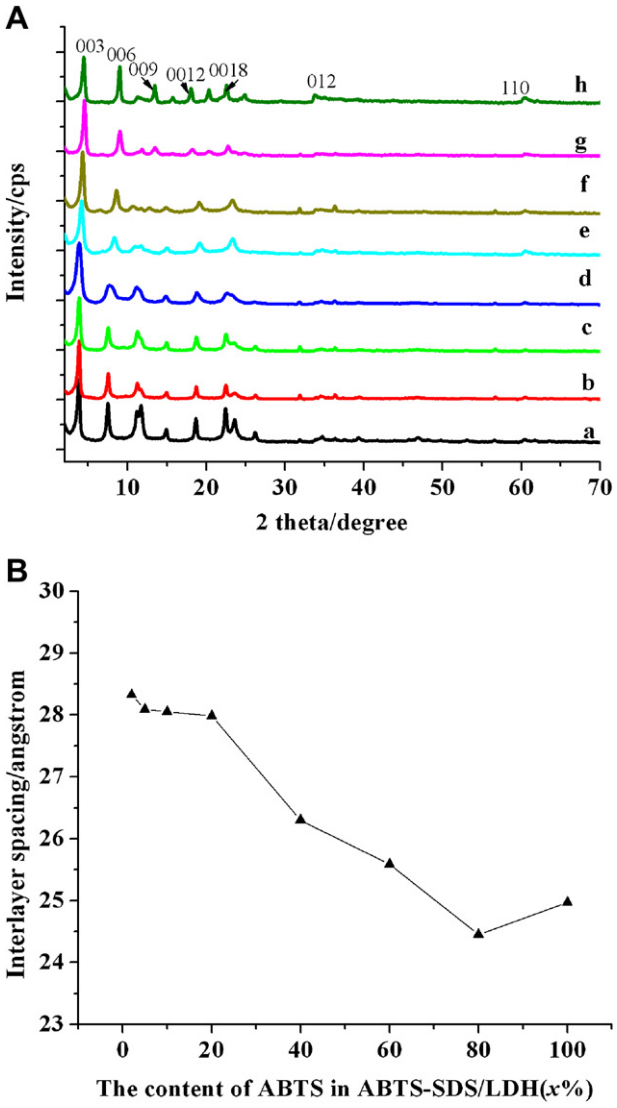

Fig. 2. (A) Powder XRD patterns of ABTS–SDS(x)/LDH. (a–h, x = 2%, 5%, 10%, 20%, 40%, 60%, 80%, 100%, respectively). (B) The plot of interlayer spacings *vs*. ABTS concentration.

2. Experimental section

2.1. Materials

Diammonium 2,2′-Azino-bis(3-ethylbenzothiazoline-6-sulfonate) (ABTS) was purchased from Sigma–Aldrich (Shanghai) Trading Co. Ltd. NaOH (AR), $Zn(NO_3)_2{\cdot}6H_2O$ (AR), $Al(NO_3)_3{\cdot}9H_2O$ (AR) and sodium 1-dodecanesulfonate (SDS, >97%) were purchased from the Beijing Chemical Co. Limited, and used without further purification. The carbonate-free deionized water was used throughout the experimental processes.

2.2. Synthesis of ABTS–SDS(x)/LDH

The co-intercalated ABTS–SDS(x)/Zn_2Al-LDH were prepared by a hydrothermal co-precipitation method as follows: $Zn(NO_3)_2{\cdot}6H_2O$ (0.4284 g, 1.44 mmol), $Al(NO_3)_3{\cdot}9H_2O$ (0.2701 g, 0.72 mmol), SDS (a mmol) and ABTS (b mmol, $a + b = 1.5$ mmol) were dissolved in 100 mL aqueous solution, and the pH value was adjusted to 7.0 by slowly adding NaOH (0.5 M) aqueous solution under N_2 atmosphere. The value x stands for the initial molar percentage of ABTS in ABTS and SDS ($x = b/(a + b) \times 100\%$; a:b = 49:1, 19:1, 9:1, 4:1, 3:2, 2:3, 1:4 and 0:1). The aqueous solution mixture was aged in an autoclave at 130 °C for 24 h. All the products were washed with hot distilled water and anhydrous ethanol several times until the filtrate was colorless, and then dried in a vacuum at 60 °C for 12 h.

2.3. Fabrication of the ABTS–SDS/LDH thin films

The film of ABTS–SDS/LDH was prepared by a solvent evaporation method: a suspension of the as-prepared ABTS–SDS/LDH powder in ethanol (1 mg/mL) was ultrasonically dispersed and then spread on a quartz or ITO substrate which was previously cleaned thoroughly by an ultrasonic anhydrous ethanol bath.

2.4. Characterization

The XRD measurements were performed on a Rigaku XRD-6000 diffractometer, using Cu-Kα radiation (λ = 0.15418 nm) at 40 kV, 30 mA, with a scanning rate of 10° min^{-1}, and the 2θ angle ranging from 3 to 70°. Fourier-transfer infrared (FT-IR) spectra were

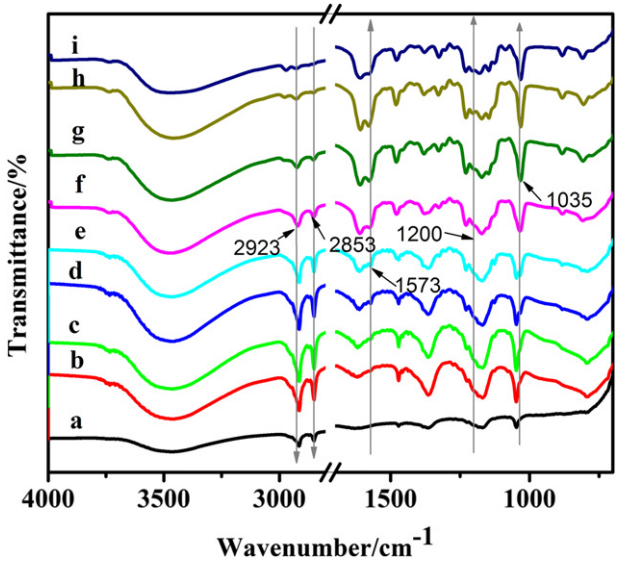

Fig. 3. FT-IR spectra of ABTS–SDS(x)/LDH (a–i, x = 0%, 2, 5%, 10%, 20%, 40%, 60%, 80%, 100%).

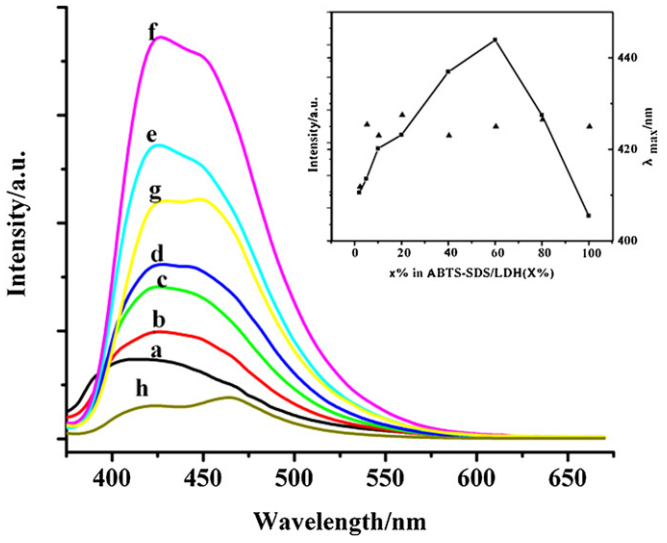

Fig. 4. The photoemission spectra of ABTS–SDS(x)/LDH with the excitation wavelength of 358 nm. The inset plot shows the fluorescence intensity and the maximum emission wavelength varying with the increase of ABTS content in the ABTS–SDS(x)/LDH (a-h, x = 2%, 5%, 10%, 20%, 40%, 60%, 80%, 100%).

recorded on a Bruker Vector 22 using the KBr disk method in the range from 4000 to 400 cm^{-1}, with a resolution of 2 cm^{-1} and accumulation of 32 scans. Elemental analysis (Al, Zn, S) was performed by atomic emission spectroscopy with a Shimadzu ICPS-7500 instrument. C, H, N contents were determined using a Perkin Elmer Elementarvario elemental analysis instrument. Scanning electron microscope (SEM) images were obtained using a Hitachi S-4700 scanning electron microscope operating at 20 kV. The UV–vis absorption spectra were recorded on a Shimadzu U-3000 spectrophotometer in the range from 200 to 700 nm with a slit width of 1.0 nm, and $BaSO_4$ was used as a reference. The fluorescence spectra were performed on a Hitachi F-7000 FL spectrophotometer with a slit width of 3 nm, excitation at 330 nm, emission spectra of 350–650 nm, and a PMT voltage of 400 V. All the samples prepared by the co-precipitation method show irregular hexagonal morphology with similar sizes, and were measured with the same volume fraction. Fluorescent lifetime measurements were recorded with an Edinburgh Instruments FL 900 fluorimeter. The percentage contribution of each lifetime component to the total decay was calculated with the Edinburgh F900 instruments software. Steady-state polarized photoluminescence measurements were recorded with an Edinburgh Instruments' FLS 920 fluorimeter. A CHI 660B electrochemical workstation (Shanghai Chenhua Instrument Co., China) was utilized for electrochemical measurements. A conventional three-electrode cell was used, including a modified ITO electrode as the working electrode, a platinum wire as the counter and an Ag/AgCl (3 M KCl) as the reference electrode. The solutions were prepared with Milli-Q water (>18 MΩcm) and purged with highly purified nitrogen for at last 10 min prior to measurement, and a nitrogen atmosphere was maintained during the electrochemical measurements. All measurements were performed at room temperature.

Table 1
Chemical compositions of ABTS–SDS/LDH (x) with different ABTS content.

Initial x	Chemical composition	Zn/Al ratio	Final x
2%	$Zn_{0.747}Al_{0.252}(OH)_2ABTS_{0.004}SDS_{0.244}\cdot 2.21H_2O$	2.96	1.61%
5%	$Zn_{0.762}Al_{0.238}(OH)_2ABTS_{0.009}SDS_{0.220}\cdot 2.34H_2O$	3.20	3.93%
10%	$Zn_{0.763}Al_{0.236}(OH)_2ABTS_{0.015}SDS_{0.206}\cdot 1.87H_2O$	3.23	6.79%
20%	$Zn_{0.756}Al_{0.243}(OH)_2ABTS_{0.027}SDS_{0.189}\cdot 2.15H_2O$	3.11	12.50%
40%	$Zn_{0.741}Al_{0.259}(OH)_2ABTS_{0.062}SDS_{0.135}\cdot 2.83H_2O$	2.86	31.47%
60%	$Zn_{0.734}Al_{0.266}(OH)_2ABTS_{0.095}SDS_{0.076}\cdot 3.21H_2O$	2.76	55.56%
80%	$Zn_{0.743}Al_{0.257}(OH)_2ABTS_{0.114}SDS_{0.029}\cdot 2.97H_2O$	2.89	79.72%
100%	$Zn_{0.750}Al_{0.270}(OH)_2ABTS_{0.135}\cdot 3.18H_2O$	2.78	100%

3. Results and discussion

3.1. Characterization of ABTS–SDS(x)/LDH

The XRD patterns of the as-prepared ABTS–SDS(x)/LDH powder samples are shown in Fig. 2A, in which x stands for the initial molar percentage of ABTS accounting for the summation of ABTS and SDS. In each case, the XRD pattern exhibits the characteristic reflections of the LDH layered structure with a series of *00l* peaks showing narrow, strong lines at low angle. The interlayer spacing can be calculated from averaging the positions of the three harmonics: $c = (1/3)(d_{003} + 2d_{006} + 3d_{009})$. It can be observed from Fig. 2B that the interlayer spacing of ABTS–SDS/LDH decreases at first from 28.32 Å (x = 2%) to the minimum 24.45 Å (x = 80%), and then

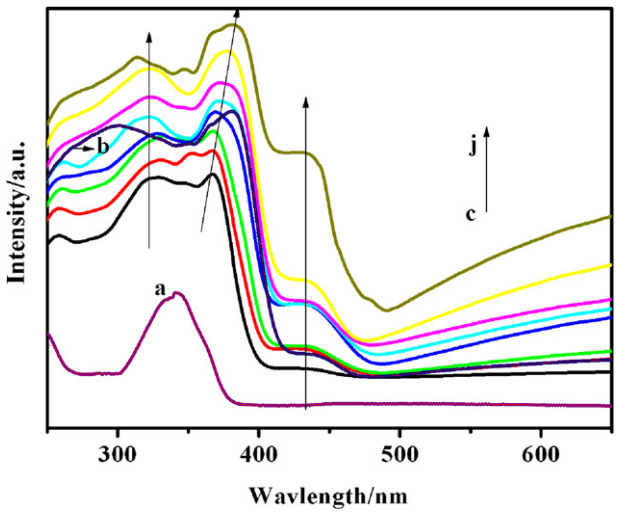

Fig. 5. The UV–vis absorption spectra of (a) ABTS (5×10^{-5} M) aqueous solution, (b) ABTS powder, (c–j) ABTS–SDS(x)/LDH powder (x = 2%, 5%, 10%, 20%, 40%, 60%, 80%, 100%).

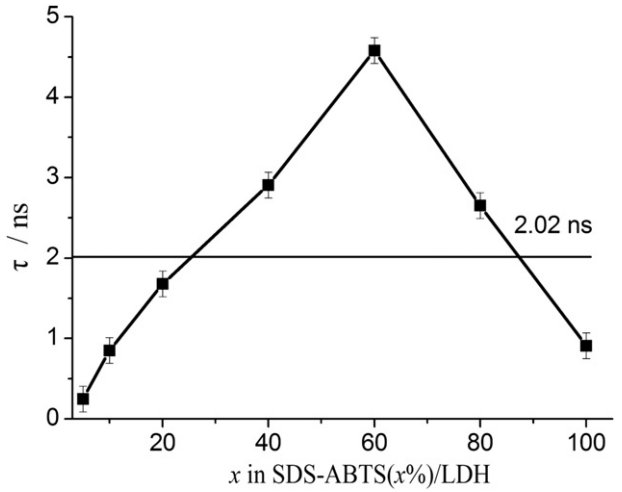

Fig. 6. The dependence of fluorescence lifetime of ABTS powder and ABTS–SDS(x)/LDH (x = 5%, 10%, 20%, 40%, 60%, 80%, 100%).

increases gradually to the 24.97 Å (x = 100%). The variation of the interlayer spacing can be attributed to the different arrangements of interlayer guest molecules with different ratios of SDS to ABTS.

The successful co-intercalation of the ABTS and SDS anions can be further confirmed by their FT-IR spectra as shown in Fig. 3. The characteristic absorption peaks at 2923 and 2853 cm^{-1} are assigned to the asymmetric $\nu_{as}(CH_2)$ and symmetric $\nu_s(CH_2)$ vibration bands of SDS while the vibrations at ~1200 and 1035 cm^{-1} are due to the O═S═O stretching vibration of the sulfonate group. Moreover, the intensity ratio of the vibrational peak of ν_{as} (CH_2) at 2923 cm^{-1} in SDS to ν_s (N═C) at 1573 cm^{-1} in ABTS decreases upon the increasing x from 2% to 100%.

The chemical compositions of products corresponding to different initial normal concentrations are tabulated in Table 1. Most of the experimental ratios of ABTS to SDS in ABTS–SDS/LDH are close to their initial nominal ratios as expected, and it increases upon the increase of initial ABTS concentration. Moreover, it can be seen that most of the molar ratios of Zn to Al deviate from the initial value of 2.0 and have a trend to be close to 3.0, which may be attributed to the difference in the dissolution equilibrium between $Zn(OH)_2$ and $Al(OH)_3$ in the LDH host layer during the hydrothermal synthesis. The similar phenomenon has also been observed in other dye intercalated Mg–Al–LDH systems [26].

3.2. Optimal luminous properties of ABTS–SDS(x)/LDH

The fluorescence emission spectra for ABTS–SDS/LDH samples with different molar ratios of ABTS to SDS are shown in Fig. 4. The fluorescence intensity of these samples increases to a maximum

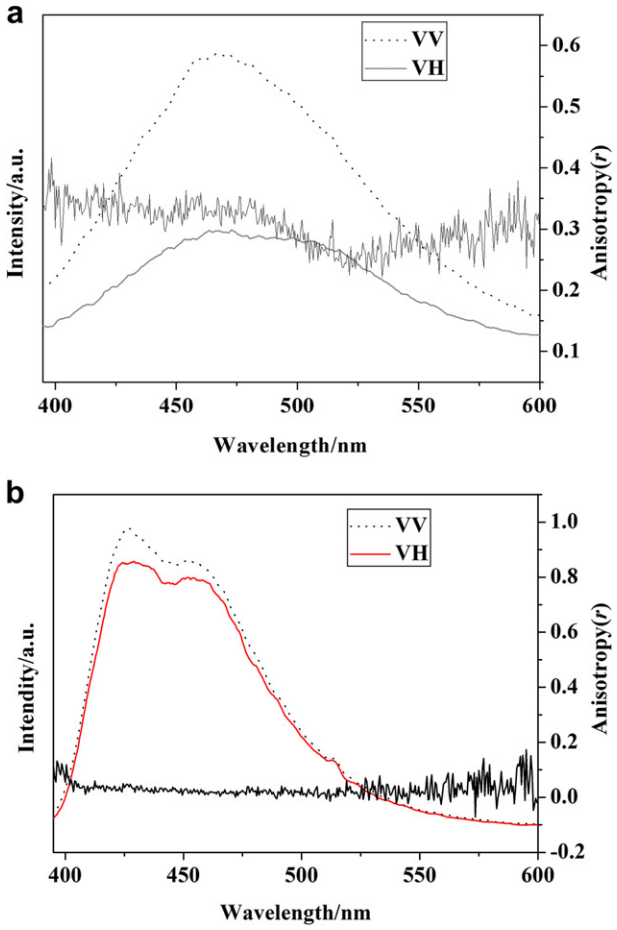

Fig. 8. Polarized fluorescence profiles in the VV, VH modes and anisotropic value (r) for a) the ABTS–SDS(60%)/LDH thin film sample and b) the ABTS solution.

(x = 60%) firstly, and then decreases with the increase of the ABTS content (inset plot of Fig. 4). The optimal luminous intensity presents in the sample with 60% initial concentration of ABTS, in which the emission peak appears at 425 nm (the S_1–S_0 transition) with the full wave at half maximum (FWHM) of *ca.* 83 nm. The maximum emission intensity decreases quickly when the initial ABTS content increases to 80%. This behavior can be attributed to the change in the state of interlayer ABTS molecule. The dye exhibits a single molecular luminescence with low ABTS concentrations, accounting for the increase in the luminous intensity firstly, and the *J*- or *H*-type dye aggregation forms when the content of ABTS increases to a certain concentration, resulting in the red shift of emission spectra and the fluorescence quenching.

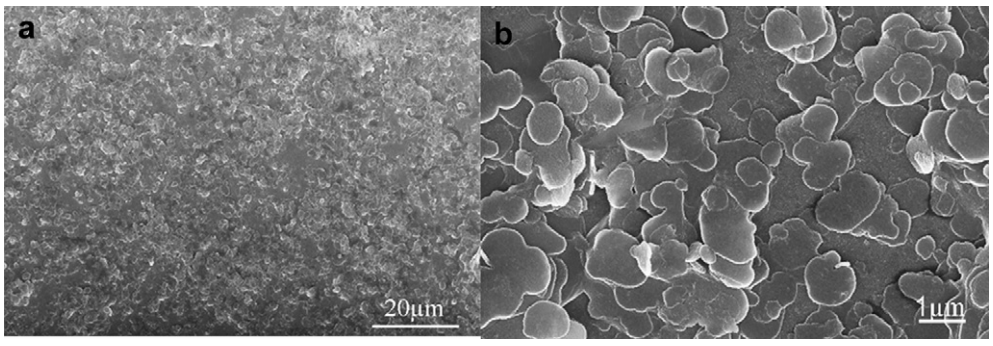

Fig. 7. SEM images for ABTS–SDS(60%)/LDH.

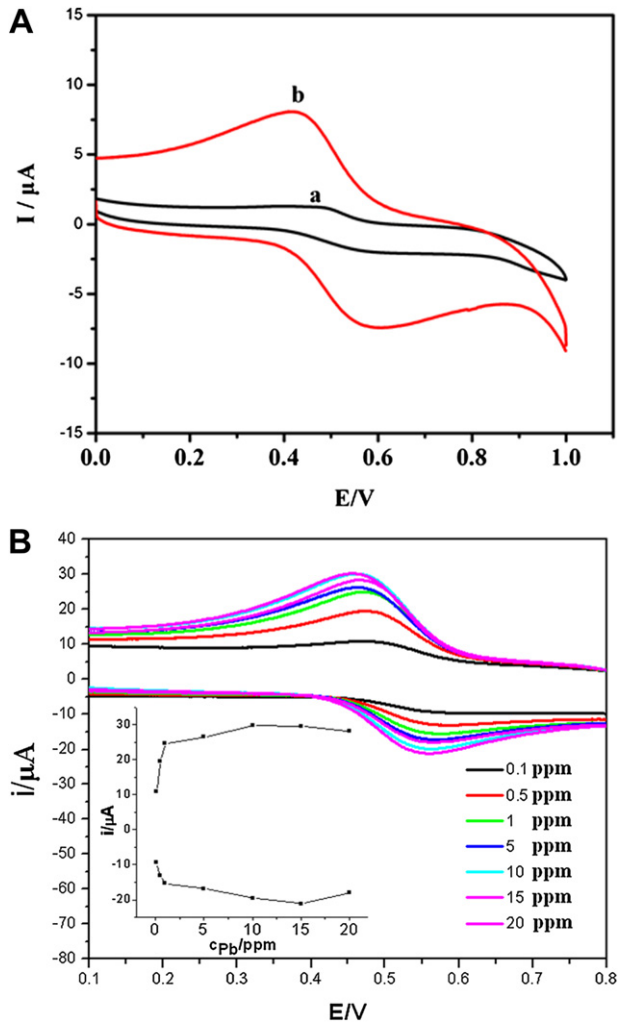

Fig. 9. (A) Cyclic voltammograms ($v = 50$ mV s^{-1}) in 0.1 M KCl electrolyte solution of (a) pure ABTS film and (b) ABTS–SDS(60%)/LDH film on ITO substrate; (B) Cyclic voltammograms ($v = 50$ mV s^{-1}) of the ABTS–SDS(60%)/LDH film under the Pb^{2+} ion aqueous solution with different concentrations.

The as-prepared ABTS–SDS(x)/LDH samples show interesting optical properties which are different from ABTS aqueous solution. Fig. 5 shows the UV–vis absorption spectra of both the ABTS solution and its solid-state phase (pristine ABTS powder and the ABTS/SDS co-intercalated LDH samples). The ABTS aqueous solution (5×10^{-5} M) exhibits a resolved absorption peaks at 340 nm. The ABTS powder presents two broad and structureless absorption bands at 300 nm and 379 nm, which can be attributed to the enhancement of intermolecular interactions, such as π–π interactions. The spectra of ABTS–SDS(x)/LDH samples have similar behaviors as the ABTS powder, indicating that dense packing of ABTS molecules occurs in the LDH layers. Upon increasing concentration of ABTS with x from 40% to 100%, the absorption peak shifts from 381 to 399 nm, suggesting the formation of the ABTS aggregations, which is consistent with their corresponding fluorescent observations.

The fluorescence and absorption spectra above clearly confirm that the introduction of SDS surfactant in the gallery of LDH enhances the emission intensity significantly compared with the sample of ABTS intercalated LDH. It was reported that surfactants or organic solvents can alter the aggregation of photoactive species [8], and the presence of the long-chain surfactant led to a high emission intensity in the system of oxazine dye intercalated cation clay [32]. In our view, the intercalated long-chain surfactant molecules achieved a nonpolar interlayer environment, which homogenously diluted and effectively isolated the interlayer ABTS molecules. As a result, the distance between dye molecules is enlarged enough for preventing the formation of aggregates. Another advantage of the surfactant molecules is that they can pre-intercalate the LDH layers for enlarging the interlayer spacing, which facilitates the intercalation of bulky dye molecules. Mohanambe et al. [33] also reported that electroneutral pyrene molecule could diffuse into the layers of MgAl–LDH after it was functionalized by anionic surfactant.

3.3. Fluorescence lifetime

To understand the excited-state properties of the ABTS–SDS(x)/LDH systems, the samples were further studied by detecting their fluorescence decays, with excitation and emission wavelength of 330 and 425 nm, respectively. The fluorescence lifetimes were obtained by fitting the decay profiles with double-exponential form. The fitting results for the decay profiles are shown in Fig. S1 in Supporting information, and the evolution of the average lifetime ($<\tau>$ [26]) on the increase of ABTS concentration is shown in Fig. 6.

Compared with the ABTS powder (*ca.* 0.35 ns), the ABTS–SDS/LDH samples exhibit tumble fluorescence lifetime from 0.25 to 4.58 ns with x value in the range 5% ~ 100%. The fluorescence lifetime of the samples with $x = 80\%$ and 100% become shorter than that with $x = 60\%$, due to the formation of aggregation as indicated by the results of fluorescence and absorption spectra. Moreover, the longest fluorescence lifetime presents in the sample of ABTS–SDS(60%)/LDH. Ray *et al.* [34] suggested that two lifetime values can be attributed to the monomers and dimers or higher aggregates, respectively. In this ABTS–SDS/LDH system, the long lifetime possibly corresponds to the intercalated ABTS in the gallery of LDH, and the short one is attributed to the adsorbed ABTS at the surface of LDH particles, since the intercalated ABTS molecule confined between the sheets is more stably immobilized.

3.4. Polarized fluorescence of the ABTS–SDS/LDH film

Fig. 7 displays the SEM images of the ABTS–SDS(60%)/LDH film. Both the low and high resolution SEM images reveal that the as-prepared LDH film are well *c*-oriented with regular LDH particles parallel to the substrate. The well-oriented ABTS–SDS/LDH film further enlightens us to study the fluorescence polarization property of the ABTS–SDS/LDH sample, and the anisotropic value r was measured. r can be expressed as the formula [35]:

$$\gamma = \frac{I_{VV} - GI_{VH}}{I_{VV} + 2GI_{VH}} \quad (1)$$

$G = I_{HV}/I_{HH}$, I_{VH} stands for the PL intensity obtained with vertical polarized light excitation and horizontal polarization detection, and I_{VV}, I_{HH}, I_{HV} are defined in a similar way. Theoretically, the value of r is in the range from −0.2 (absorption and emission transition dipoles are perpendicular to one another) to 0.4 (two transition dipoles are parallel to each other). The typical measurement setup of polarized fluorescence was employed to determine the fluorescence anisotropic value r, and the excitation and emission light keep 45° with respect to the film. The polarized photoemission spectra of the ABTS–SDS/LDH film is displayed in Fig. 8. It was observed that the ABTS–SDS(60%)/LDH thin film shows well-defined blue fluorescence anisotropy between the parallel and perpendicular to the excitation polarized direction (I_{VV} vs. I_{VH}). The anisotropic value (r) is *ca.* 0.35 at 425 nm (Fig. 8a), whereas the ABTS solution is nearly 0 (Fig. 8b), demonstrating the uniform dispersion and well-oriented ABTS anions in the galleries of LDH.

Moreover, the uniform r value ranging in 360–600 nm indicates that polarization scrambling via π–π interaction is minimal within the thin film.

3.5. Electrochemistry characteristics

To further study the electrochemical behaviors of the ABTS–SDS(60%)/LDH film, cyclic voltammogram measurements were performed on both the ABTS–SDS(60%)/LDH and pure ABTS dye films. Compared with that of the pure ABTS (Fig. 9A(a)), the ABTS–SDS(60%)/LDH film shows a well-defined electrochemical response, with the two peaks ($E_{onset,red}$ and $E_{onset,ox}$) located at *ca.* 0.47 and 0.56 V (Fig. 9A(b)), respectively, corresponding to the reversible reduction and oxidation of the electroactive center of the ABTS immobilized between the LDH layers. Moreover, the ABTS–SDS(60%)/LDH film also exhibits electrochemical response to the aqueous solution with different Pb^{2+} concentrations (Fig. 9b). It can be observed that the reduction and oxidation peak currents show a good linear relationship ($R^2 = 0.984$) with the concentration of the Pb^{2+} in the range from 0.1 to 1 ppm. When the Pb^{2+} concentration further increase from 1 to 20 ppm, the peak currents gradually achieve a constant due to the saturation of the electroactive center of ABTS–SDS(60%)/LDH film. These results demonstrate the ABTS–SDS(60%)/LDH film can detect trace amount of Pb^{2+} ion in aqueous solution, which may have potential application in the field of electrochemical ion-probe. As an example, the ABTS–SDS(60%)/LDH film exhibit a high detection accuracy of the aqueous solution containing 0.2 ppm of Pb^{2+} ion (Supporting information: Fig. S2).

4. Conclusions

In summary, the photoluminescent properties of ABTS dye and SDS co-intercalated Zn–Al–LDH for both powder and film samples have been investigated. Compared with the ABTS powder, the fluorescence lifetime of ABTS–SDS/LDH ($x = 10$–100%) composites increases greatly. The brightest luminous intensity and the longest fluorescence lifetime present in the ABTS–SDS(60%)/LDH sample, demonstrating that the immobilization of ABTS anions between the rigid LDH galleries can suppress the nonradiative relaxation process effectively. Moreover, The thin film ABTS–SDS(60%)/LDH shows well-defined polarized luminescence with the fluorescence anisotropy of *ca.* 0.35. The ABTS–SDS(60%)/LDH film also exhibits good electrochemical response to Pb^{2+} ion in the aqueous solution. Therefore, the as-prepared film based on an organic dye anions regularly arranged within an inorganic LDH matrix may serve as one new type of lamellar organic–inorganic material with interesting luminescent properties and electrochemical activity.

Acknowledgments

This work was supported by the National Natural Science Foundation of China, the 111 Project (Grant No.: B07004) and the 973 Program (Grant No.:2011CBA00504), and the Fundamental Research Funds for the Central Univerisities.

Appendix. Supporting information

Supplementary material associated with this article can be found, in the online version, at doi:10.1016/j.dyepig.2011.11.004.

References

[1] Zhang Q, Atay T, Tischler JR, Bradley MS, Bulovi V, Nurmikko1 AV. Highly efficient resonant coupling of optical excitations in hybrid organic/inorganic semiconductor nanostructures. Nature Nanotechnology 2007;2:555–9.
[2] Agranovich VM, Gartstein YN, Litinskaya M. Hybrid resonant organic–inorganic nanostructures for optoelectronic applications. Chemical Review; 2011. doi:10.1021/cr100156x.
[3] Yan D, Lu J, Ma J, Qin S, Wei M, Evans DG, et al. Layered host–guest materials with reversible piezochromic luminescence. Angewandte Chemie International Edition 2011;50:7037–40.
[4] Guerrero-Martínez A, Fibikar S, Pastoriza-Santos I, Liz-Marzán LM, De Cola L. Microcontainers with fluorescent anisotropic zeolite L cores and isotropic silica shells. Angewandte Chemie International Edition 2009;48:1266–70.
[5] Cucinotta F, Popović Z, Weiss EA, Whitesides GM, De Cola L. Microcontact transfer printing of zeolite monolayers. Advanced Materials 2009;21:1142–5.
[6] Zhou CH, Shen ZF, Liu LH, Liu SM. Preparation and functionality of clay-containing films. Journal of Material Chemistry; 2011. doi:10.1039/C1JM11479D.
[7] Carbonaro CM, Anedda A, Grandi S, Magistris AJ. Hybrid materials for solid-state dye laser applications. Journal of Physical Chemistry B 2006;110:12932–7.
[8] Ogawa M, Kuroda K. Photofunctions of intercalation compounds. Chemical Review 1995;95:399–438.
[9] Costantino U, Nocchetti M. In: Rives V, editor. Layered double hydroxides: present and future. New York: Nova Science Publications; 2001 [Ch. 12.9].
[10] Guo X, Zhang F, Evans DG, Duan X. Layered double hydroxide films: synthesis, properties and applications. Chemical Communications 2010;46:5197–210.
[11] Newman SP, Jones W. Synthesis, characterization and applications of layered double hydroxides containing organic guests. New Journal of Chemistry 1998;22:105–15.
[12] Wang Y, Yang W, Chen C, Evans DG. Fabrication and electrochemical characterization of cobalt-based layered double hydroxide nanosheet thin-film electrodes. Journal of Power Sources 2008;184:682–90.
[13] Wang CJ, Wu YA, Jacobs RMJ, Warner JH, Williams GR, O'Hare D. Reverse micelle synthesis of Co–Al LDHs: control of particle size and magnetic properties. Chemistry of Materials 2011;23:171–80.
[14] Fogg AM, Green VM, Harvey HG, O'Hare D. New separation science using shape-selective ion exchange intercalation chemistry. Advanced Materials 1999;11:1466–9.
[15] Wang Y, Zhang D, Tang M, Xu S, Li M. Electrocatalysis of gold nanoparticles/layered double hydroxides nanocomposites toward methanol electrooxidation in alkaline medium. Electrochimica Acta 2010;55:4045–9.
[16] Wang J, Zhao L, Shi H, He J. Highly enantioselective and efficient asymmetric epoxidation catalysts: inorganic nanosheets modified with α-amino acids as ligands. Angewandte Chemie International Edition; 2011. doi:10.1002/anie.201103713.
[17] Wang J, Zhou J, Li Z, Song Y, Liu Q, Jiang Z, et al. Magnetic, luminescent Eu-doped Mg–Al layered double hydroxide and its intercalation for ibuprofen. Chemistry–A European Journal 2010;16:14404–11.
[18] Yan D, Lu J, Wei M, Han J, Ma J, Li F, et al. Ordered poly(*p*-phenylene)/layered double hydroxide ultrathin films with blue luminescence by layer-by-Layer assembly. Angewandte Chemie International Edition 2009;48:3073–6.
[19] Nie HQ, Hou WG. Methods and applications for delamination of layered double hydroxides. Acta Physico–Chimica Sinica 2011;27:1783–96.
[20] Kameyama T, Okazaki K, Takagia K, Torimoto T. Stacked-structure-dependent photoelectrochemical properties of CdS nanoparticle/layered double hydroxide (LDH) nanosheet multilayer films prepared by layer-by-layer accumulation. Physical Chemistry Chemical Physics 2009;11:5369–76.
[21] Tang P, Feng Y, Li D. Fabrication and properties of Acid Yellow 49 dye-intercalated layered double hydroxides film on an alumina-coated aluminum substrate. Dyes and Pigments 2011;91:120–5.
[22] Xu J, Zhao S, Han Z, Wang X, Song YF. Layer-by-Layer assembly of $Na_9[EuW_{10}O_{36}]\cdot 32H_2O$ and layered double hydroxides leading to ordered ultrathin films: cooperative effect and orientation effect. Chemistry–A European Journal 2011;17:10365–71.
[23] Yan D, Lu J, Wei M, Evans DG, Duan X. Recent advances in photofunctional guest/layered double hydroxide host composite systems and their applications: experimental and theoretical perspectives. Journal of Material Chemistry 2011;21:12128–39.
[24] Bauer J, Behrens P, Speckbacher M, Langhals H. Composites of perylene chromophores and layered double hydroxides: direct synthesis, characterization, and photo- and chemical stability. Advanced Functional Materials 2003;13:241–8.
[25] Gago S, Costa T, de Melo JS, Gonçalves IS, Pillinger M. Preparation and photophysical characterization of Zn–Al layered double hydroxides intercalated by anionic pyrene derivatives. Journal of Material Chemistry 2008;18:894–904.
[26] Yan D, Lu J, Wei M, Evans DG, Duan X. Sulforhodamine B intercalated layered double hydroxide thin film with polarized photoluminescence. The Journal of Physical Chemistry B 2009;113:1381–8.
[27] Tang P, Feng Y, Li D. Improved thermal and photostability of an anthraquinone dye by intercalation in a zinc-aluminium layered double hydroxide host. Dyes and Pigments 2011;90:253–8.
[28] Yan D, Lu J, Wei M, Qin S, Chen L, Zhang S, et al. Heterogeneous transparent ultrathin films with tunable-color luminescence based on the assembly of

photoactive organic molecules and layered double hydroxides. Advanced Functional Materials 2011;21:2497–505.
[29] Pinkernell U, Nowack B, Gallard H, Von Gunten U. Methods for the photometric determination of reactive bromine and chlorine species with ABTS. Water Research 2000;34:4343–50.
[30] Pietta P, Simonetti P, Mauri P. Antioxidant activity of selected medicinal plants. Journal of Agricultural and Food Chemistry 1998;46: 4487–90.
[31] Therias S, Mousty C, Forano C, Besse JP. Electrochemical transfer at anionic clay modified electrodes-case of 2,2'-Azinobis(3-ethylbenzothiazoline-6-sulfonate). Langmuir 1996;12:4914–20.
[32] Bujdák J, Iyi N. Spectral and structural characteristics of oxazine 4/hexadecyltrimethylammonium montmorillonite films. Chemistry of Materials 2006;18:2618–24.
[33] Mohanambe L, Vasudevan S. Aromatic molecules in restricted geometries: pyrene excimer formation in an anchored bilayer. The Journal of Physical Chemistry B 2006;110:14345–54.
[34] Ray K, Nakahara H. Adsorption of sulforhodamine dyes in cationic Langmuir–Blodgett films: spectroscopic and structural studies. The Journal of Physical Chemistry B 2002;106:92–100.
[35] Valeur B. Molecular fluorescence: principles and applications. Verlag GmbH: Wiley-VCH; 2001.